CrossMark

RESEARCH ARTICLE

Holocene phreatomagmatic eruptions alongside the densely populated northern shoreline of Lake Kivu, East African Rift: timing and hazard implications

Sam Poppe [1] · Benoît Smets [1,2,3] · Karen Fontijn [4] · Montfort Bagalwa Rukeza [5] ·
Antoine De Marie Fikiri Migabo [5] · Albert Kyambikwa Milungu [5] ·
Didier Birimwiragi Namogo [5] · François Kervyn [3] · Matthieu Kervyn [1]

Abstract The Virunga Volcanic Province (VVP) represents the most active zone of volcanism in the western branch of the East African Rift System. While the VVP's two historically active volcanoes, Nyamulagira and Nyiragongo, have built scoria cones and lava flows in the adjacent lava fields, several small phreatomagmatic eruptive centers lie along Lake Kivu's northern shoreline, highlighting the potential for explosive magma-water interaction. Their presence in the densely urbanized Sake-Goma-Gisenyi area necessitates an assessment of their eruptive mechanisms and chronology. Some of these eruptive centers possess multiple vents, and depositional contacts suggest distinct eruptive phases within a single structure. Depositional facies range from polymict tuff breccia to tuff and loose lapilli, often impacted by blocks and volcanic bombs. Along with the presence of dilute pyroclastic density current (PDC) deposits, indicators of magma-water interaction include the presence of fine palagonitized ash, ash aggregates, cross-bedding, and ballistic impact sags. We estimate that at least 15 phreatomagmatic eruptions occurred in the Holocene, during which Lake Kivu rose to its current water level. Radiocarbon dates of five paleosols in the top of volcanic tuff deposits range between ~2500 and ~150 cal. year BP and suggest centennial- to millennial-scale recurrence of phreatomagmatic activity. A vast part of the currently urbanized zone on the northern shoreline of Lake Kivu was most likely impacted by products from phreatomagmatic activity, including PDC events, during the Late Holocene, highlighting the need to consider explosive magma-water interaction as a potential scenario in future risk assessments.

Editorial responsibility: P-S Ross

✉ Sam Poppe
  sam.poppe@vub.ac.be

1 Department of Geography, Earth System Science, Vrije Universiteit Brussel, Pleinlaan 2, 1050 Brussels, Belgium

2 European Center for Geodynamics and Seismology, 19 Rue Josy Welter, 7256 Walferdange, Grand Duchy, Luxembourg

3 Department of Earth Sciences, Royal Museum for Central Africa, 13 Leuvensesteenweg, 3080 Tervuren, Belgium

4 Department of Earth Sciences, University of Oxford, South Parks Road, Oxford OX1 3AN, UK

5 Goma Volcano Observatory, 142 Avenue Rond-Point, Goma, Democratic Republic of the Congo

Introduction

Although the Virunga Volcanic Province (VVP) is mostly known for its effusive volcanism, the presence of phreatomagmatic centers with a young morphology along Lake Kivu's densely populated northern shoreline signals the need to consider the future hazard of explosive magma-water interactions. The VVP lies at a transfer zone that separates two rift segments (i.e., Kivu and Albert rifts; Ebinger 1989; Smets et al. 2016) within the western branch of the East African Rift (Fig. 1a, b). The VVP hosts eight large volcanic edifices, of which Nyiragongo and Nyamulagira, in the western, intra-rift part of the VVP, have frequently erupted over the past 150 years. Nyamulagira is a flow-dominated
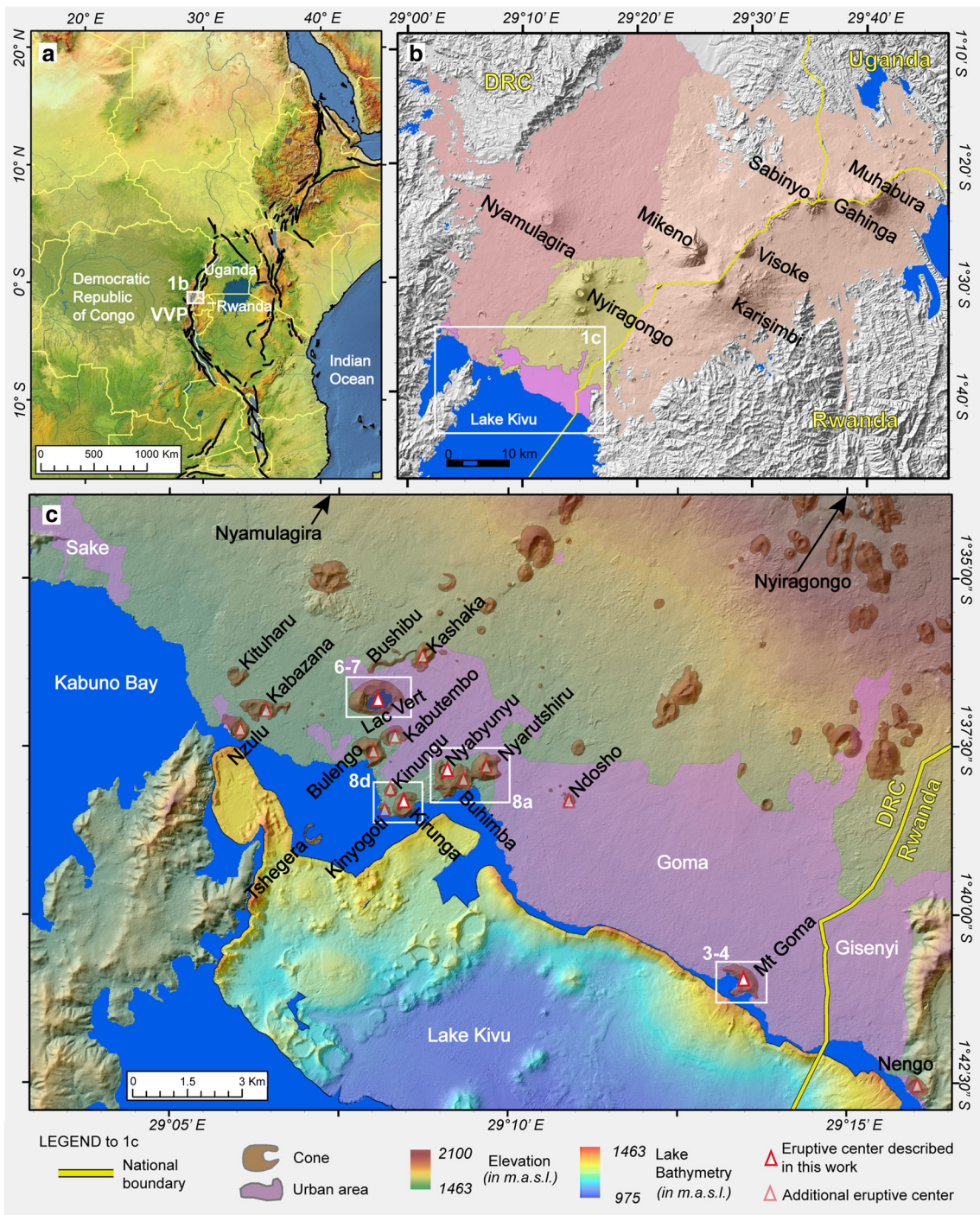
Fig. 1 **a** Location of the Virunga Volcanic Province (*VVP*) in the western branch of the East African Rift; major faults are marked in *black*, international borders in *yellow*. **b** Hillshade relief image of the VVP based on the SRTM digital elevation model (*DEM*) at 30 m resolution (www.usgs.gov); the active volcanoes and their adjacent lava flow fields of Nyamulagira (*red field*) and Nyiragongo (*yellow field*) lie within the rift valley, six dormant VVP volcanoes lie on the rift shoulder (*pink field*); international borders are marked in *yellow*, the Saké-Goma-Gisenyi urban area houses >1.2 million people (*purple area*). **c** SRTM-derived hillshade relief image of the northern shoreline of Lake Kivu and bathymetry of the Lake Kivu floor (from Ross et al. 2014); *white boxes* mark the positions of Figs. 3, 5, and 6

shield volcano (e.g., Smets et al. 2015). Nyiragongo is a stratovolcano complex with a semi-permanent lava lake (Fig. 1; e.g., Tazieff 1977; Komorowski et al. 2003). Both edifices' flanks and their adjacent lava fields are occupied by >200 satellite eruptive centers, most of which are scoria cones. The southernmost centers along the northern shoreline of Lake Kivu stand out due to their poorly documented phreatomagmatic nature (Fig. 1).

Denaeyer (1975) provided morphological and preliminary stratigraphic descriptions of the satellite center deposits along Lake Kivu's northern shoreline, and Tuttle et al. (1990) suggested these deposits represent a potential explosive eruptive hazard in the area, based on stratigraphic facies and two radiocarbon dates (740 ± 110 and 10,240 ± 30 years BP; Table 1). Capaccioni et al. (2003) present a geochemical study of some of the small eruptive centers and suggest a petrogenetic relationship between the magma which fed these centers and the highly alkaline, silica-undersaturated magmas which feed Nyiragongo's main edifice. These studies recognize the phreatomagmatic nature of most eruptive centers within a 2-km distance of the lake shore, in contrast to the dry magmatic nature of the centers further up the main edifices' flanks. The presence of >1.2 million inhabitants in the Sake-Goma-Gisenyi urban area (Fig. 1c) necessitates a detailed hazard assessment based on stratigraphic descriptions and absolute chronology of the phreatomagmatic deposits.

In this study, we identify evidence of explosive magma-water interaction in key lithofacies of the small eruptive centers along the northern shoreline of Lake Kivu. We further propose more detailed eruptive scenarios for the two best exposed complexes, Mt. Goma and Lac Vert (Fig. 1), and provide a radiocarbon chronology of phreatomagmatic eruptions in the area, put into the context of Holocene lake-level variations of Lake Kivu. Finally, we discuss the implications for this phreatomagmatic hazard in the densely populated Sake-Goma-Gisenyi urban area.

Table 1 Measured and calibrated radiocarbon ages defined from paleosols and shell material at stratigraphical boundaries in phreatomagmatic small eruptive centers on the northern shoreline of Lake Kivu

Sample	Beta analytic lab code	Sample type and stratigraphic relation	Measured ^{14}C age (year BP)	Calibrated mean age (a cal. BP ± 1σ)	Calibrated age range 2σ (a cal. BP)	^{13}C/^{12}C (±0.5 ‰)
13KIR801	371363	Paleosol in top deposits of Kirunga	60 ± 30	117 ± 77	*31–139 (72.3 %); 222–258 (23.1 %)*	−25.9
13KIR0701	371362	Paleosol in top deposits of Kirunga	340 ± 30	395 ± 51	*311–481 (100%)*	−27.3
Lk-89-04[a]	N/A	Charcoal in top deposits of Mt. Goma—phase 3	740 ± 110	703 ± 97	*539–834 (86.7 %); 842–910 (8.7 %)*	–
13MGO190202	371354	Paleosol in top deposits of Mt. Goma—phase 3	650 ± 30	611 ± 37	*556–607 (51.9 %); 625–670 (43.5 %)*	−23.5
13MGO190201	371353	Paleosol in top deposits of Mt. Goma—phase 3	840 ± 30	749 ± 37	*686–797 (95.0 %); 888–891 (0.4 %)*	−24.3
13LVE1201	371355	Paleosol in top deposits of Lac Vert—phase 2	310 ± 30	382 ± 47	*301–465 (100%)*	−18.9
13LVE1301	371356	Paleosol in top deposits of Lac Vert—phase 2	300 ± 30	378 ± 48	*296–340 (25.8 %); 347–461 (69.6 %)*	−19.7
14LVE1002[a]	386922	Paleosol in top deposits of Lac Vert—phase 2	640 ± 30	608 ± 35	*554–610 (54.4 %); 621–668 (41.0 %)*	−20.0
14LVE1002b	386921	Paleosol in top deposits of Lac Vert—phase 2	690 ± 30	638 ± 40	*562–593 (26.5 %); 638–685 (68.9 %)*	−22.1
13LVE240202[a]	371,366	Terrestrial gastropod shell in top deposits of Lac Vert—phase 1	1120 ± 30	1024 ± 43	*956–1088 (91.8 %); 1109–1124 (1.4 %); 1135–1141 (0.5 %); 1160–1173 (1.7 %)*	−10.5
13LVE240202b	371367	Paleosol in shell in top deposits of Lac Vert—phase 1	2140 ± 30	2142 ± 78	*2006–2026 (3.2 %); 2037–2162 (71.2 %); 2169–2179 (1.5 %); 2244–2302 (19.5 %)*	−21.4
13LVE1402	371358	Paleosol in top deposits of Lac Vert—phase 1	2320 ± 30	2334 ± 37	*2184–2235 (5.3 %); 2306–2378 (90.1 %)*	−17.6
13NYAB0501	371364	Paleosol in top deposits of Nyabyunyu	850 ± 30	761 ± 42	*690–799 (90.2 %); 870–898 (5.2 %)*	−21.5
13NYAB0401	371365	Paleosol in top deposits of Nyabyunyu	1480 ± 30	1365 ± 34	*1305–1412 (100%)*	−20.2
Lk-89-02[a]	N/A	Charcoal below the base of Nengo scoria cone	10,240 ± 30	11,972 ± 221	*11,411–11,429 (0.4 %); 11,495–11,545 (1.4 %); 11,601–12,411 (93.6 %)*	–

Samples were pretreated with HCl to remove carbonates. Dating was done at Beta Analytic, Florida, USA, by accelerator mass spectrometry and the resulting ages were calibrated using the Oxcal v4.2.3 software (Bronk Ramsey 2009) with the IntCal13 curve of Reimer et al. (2013). Outcrop locations are presented in Figs. 3, 6, and 8, with coordinates provided in Supplementary Table S1

[a] Measured ages from Tuttle et al. (1990); re-calibrated with Oxcal v4.2 and the Intcal13 curve

Phreatomagmatism: Concepts and Definitions

The term phreatomagmatism defines eruptions in which magma interacts explosively with external water (Houghton et al. 2015). External water is vaporized upon contact with ascending hot magma, which is in turn efficiently fragmentated into relatively fine-grained pyroclasts as compared with coarser fragments formed in dry magmatic eruptions during which fragmentation is driven purely by degassing of magmatic volatiles (e.g., Kokelaar 1986; Zimanowski et al. 1997). The explosivity of the magma-water interactions often results in the excavation of bedrock. Complex environmental controls at the eruptive vent can result in either simple evolution or complex back-and-forth shifting between contrasting phreatomagmatic and magmatic styles during an eruptive phase. Factors controlling the eruptive style include varying influx rates of external water, variations in magma ascent rate and patterns, and rates of magma degassing (e.g., Kokelaar 1986; Wohletz 1986; Houghton et al. 1999; Németh et al. 2012).

Mafic magma quenched rapidly by external water forms sideromelane fragments which can be recognized in thin section by their yellow-brown translucence and isotropic character. Sideromelane is often altered to form the material "palagonite," which comprises hydrated glass and smectitic clays, often associated with zeolites (e.g., Pauly et al. 2011). In the eruption plume, moist ash can aggregate into accretionary lapilli, which commonly have a concentric structure. Accretionary lapilli with a solid clast core are called armored lapilli (Fisher and Schmincke 1984).

During the 1963 Surtsey (White and Houghton 2000) and 1965 Taal (Moore et al. 1966) eruptions, small-scale phreatomagmatic eruptions occurred as a succession of intermittent explosions. The ratio of magma to water at the fragmentation locus in the vent largely controls the density and temperature of the erupted mixture of pyroclasts, magmatic gases, and water vapor (Koyaguchi and Woods 1996). The pulsating phreatomagmatic plume formed from this mixture often becomes too dense to remain buoyant in air and instead generates ground-hugging dilute pyroclastic density currents (PDC), which expand laterally away from the vent (e.g., Schmincke et al. 1973; Brand and Clarke 2012; Van Eaton et al. 2012). These types of PDCs have historically been termed base surges, but the more general term dilute PDC is preferred here (Manville et al. 2009; White and Ross 2011). The spatial extent and sedimentological features of PDC deposits, e.g., cross-bedding and dune wavelengths, help inferring the variations in the controlling factors which control PDC run-out distance (e.g., Valentine and Fischer 2000; Brand and Clarke 2012; Brand et al. 2014).

Volcanic constructs dominantly formed by explosive magma-water interaction often display a wide range of magmatic and phreatomagmatic lithofacies. Based on their morphology they are subdivided into tuff cones, tuff rings, and maars (Manville et al. 2009; Ross and White 2011).

Methodology

Two field missions were undertaken in 2013, during which volcanic deposits associated with small eruptive centers within 2 km of the Lake Kivu shoreline were described for geometry, texture, and lithological componentry. We adopt the nomenclature of volcaniclastic deposits as proposed by White and Houghton (2006). Accessibility of outcrops is typically best in populated areas where scoria and coarse ash are quarried as construction sands. Where deposits were inaccessible, we complement our observations with those of Denaeyer (1975) and Capaccioni et al. (2003). Geographic coordinates of outcrop and sample locations are given in Supplementary Table S1. Qualitative observations of clast type and componentry of representative facies were performed on thin sections.

We collected 12 paleosol samples and one gastropod shell from seven different horizons for radiocarbon dating of the most recent phreatomagmatic activity in the area (Table 1). Samples were preferentially collected from the soils in the uppermost parts of the deposits immediately below overlying, more recent lava flows. Analysis was performed at Beta Analytic Inc. (Florida, USA) using accelerator mass spectrometry. The resulting ages were calibrated in OxCal v4.2 (http://www.c14.arch.ox.ac.uk; Bronk Ramsey 2009; Table 1), using the IntCal13 calibration curve (Reimer et al. 2013).

Stratigraphy and chronology of phreatomagmatic complexes

Depositional and clast characteristics of the studied deposits at the small eruptive centers define five contrasting lithofacies, interpreted as phreatomagmatic or magmatic in origin (Table 2; Fig. 2). Using these lithofacies, we describe the complex internal stratigraphy of the two best exposed complexes, Mt. Goma and Lac Vert, as well as eruptive units at two additional cones.

The Mt. Goma tuff cone complex

Mt. Goma (MGO) is located within the city center of Goma, at the shoreline of Lake Kivu (Fig. 1). It is a complex of three to four craters, the largest of which is breached into the lake and used as the city's harbor (Fig. 3). The Mt. Goma magma has a silica-undersaturated foiditic bulk composition and is geochemically related to central Nyiragongo lavas (melilite or leucite-bearing nephelinites; Capaccioni et al. 2003). We

Table 2 Description of the four lithofacies identified in the phreatomagmatic and magmatic deposits at small eruptive centers proximal to the shoreline of Lake Kivu

Facies name	Facies description
Facies 1: polymict tuff breccia (Fig. 2a, b)	Poorly sorted; chaotic to crudely bedded; decimeter- to meter-sized blocks are lithics from pre-existing lava flows (low vesicularity, subangular shape, high amounts of different crystal types); (semi-)consolidated gray matrix consists of juvenile fine lapilli and ash (high vesicularity, angular shape, vitric) and lapilli- to ash-sized pulverized lithics
Facies 2: palagonitized tuff and lapilli tuff (Fig. 2c–f)	Consolidated beds of >50 % fine ash, 5–20 % millimeter- to centimeter-sized lithic clasts and 20–30 % of vesicular (juvenile) lapilli; armored lapilli with 0.5–3-cm-sized solid core and 1–5 mm coating of fine ash; ash aggregates; impact sags; meter-scale cross-bedding; pinch-and-swell beds; partial palagonitization of vitric ash fraction resulted in ochre-colored deposits
Facies 3a: coarse to fine tuff (Fig. 2g, h)	Centimetric alternations of poorly consolidated moderately to well-sorted coarse to fine ash with impact sags from decimeter- to meter-sized lithic ballistic blocks of pre-existing lava; small-scale cross-bedding, pinch-and-swell textures between individual beds; decimeter-deep erosion channels; chute-and-pool structures
Facies 3b: tuff and lapilli tuff (Fig. 2i, j)	Moderately consolidated and sorted centimeter-scale alternations of coarse ash and vesicular lapilli; <1 % fine ash; higher amount of vesicular juvenile clasts compared with facies 3a; bed perforations by decimeter- to meter-sized lithic blocks and vesicular volcanic bombs; chute-and-pool structures; decimeter-deep erosion channels
Facies 4: scoria, spatter and lava (Fig. 2k, l)	Highly vesicular brown to black welded lava spatter and bombs and angular lapilli; welded spatter from lava fountains; xenoliths from the crystalline basement; spatter levees along eruptive fissures; lava mounds; lava flows

distinguish three major eruptive units, based on facies characteristics and bedding dip directions (Figs. 3 and 4):

Phase MGO-P1 is exposed at the southern cliffs which are eroded by the lake waves (Fig. 4). The beds were sourced from the southernmost and smallest crater P1 (~175 m diameter) of the complex, as can be inferred from their crater-inward dip (Fig. 3). This first unit is maximum 25 m thick, divided in decimeter-scale beds of consolidated facies 2 tuff and lapilli tuff (Figs. 2c–f and 4a). The fine ash matrix is dark brown and individual particles have a yellow palagonite rim, responsible for the ochre color of the deposits (Fig. 2e, f).

Phase MGO-P2 is exposed at the summit rim and within the central subaerial crater. Crater-inward dips of the beds are consistent with this crater as their point of origin (Fig. 3). The crater has a diameter of 300–400 m and a maximum depth of 100 m. The MGO-P2 unit is minimum 10 m thick and comprises facies 3a unconsolidated fine and coarse tuffs with cross-laminations (Figs. 2 and 4b). MGO-P2 is separated from MGO-P1 to the South by a sudden upward decrease in consolidation.

MGO-P3 is the most voluminous phase and forms the entire northern part of the eruptive complex. Subaerial morphology and bedding dips suggest that the vent of origin corresponds to the bay of Goma harbor (Fig. 3). Immediately NW of the MGO-P2 crater, MGO-P3 beds truncate the MGO-P2 tuffs. The MGO-P3 subunits are each 0.5–2 m thick and alternate between facies 3a coarse-and-fine tuffs and facies 3b tuff and lapilli tuff (Fig. 2g–j). The latter facies becomes more abundant upwards in the section, as the proportion of fine ash decreases (Fig. 4c, d). Deposits are generally (sub)parallel bedded, with meter-scale undulations, pinch-and-swell and chute-and-pool structures and occasionally erosional

channels. The entire sequence contains varying amounts of subangular centimeter- to meter-sized, poorly vesicular lava blocks which contain 1–40 vol% nepheline and leucite crystals. These blocks are interpreted as accidental lithics disrupted from pre-MGO lava flows (Denaeyer 1975). The largest lithic blocks created impact sags in underlying beds in the lowermost subunits of MGO-P3, whereas lithic blocks and vesicular bombs perforated the bedding in the upper part.

A >3-km-wide sublacustrine fan extends SW from Mt. Goma to >250 m below the current lake level (Fig. 1c; Ross et al. 2014). This fan could represent either the subaqueous continuation of the complex, or a debris fan originating from a collapsed, subaerial part of Mt. Goma. Quarried sections of facies 3a tuffs of the outer flank sequence are exposed on land tens of meters away from the northern morphological base of the complex (Fig. 4e). In these quarries, the thickness of these tuffs is still >3 m. These tuffs are overlain by a ~1-m-thick lava flow, identified as the voluminous 'Buyinga' flow which covers a large part of Nyiragongo's southern flank on the map by Thonnard et al. (1965) (Fig. 4e). The extent of MGO-P3 deposits well beyond the Mt. Goma cone suggests that the subaerial cone is the summit of a much larger eruptive complex which has its base >250 m below the current lake level (Fig. 1c).

Tuttle et al. (1990) obtained an age of 703 ± 97 a cal. BP on a charcoal sample from within the top unit of the MGO-P3 tuffs (Lk-89-04; Table 1; Figs. 3 and 5). Two newly collected samples from the poorly developed paleosol above MGO-P3 and directly below the overlying Buyinga lava flow (Fig. 4e), were dated at 749 ± 37 a cal. BP (13MGO190201) and 611 ± 37 a cal. BP (13MGO190202; Table 1; Fig. 5). These

ages are consistent with the results of Tuttle et al. (1990) and suggest that the minimum eruptive age for the upper part of Mt. Goma ranges between ca. 900 and 550 a. This age also represents the oldest possible eruptive age range of the Buyinga lava flow.

The Lac Vert maar volcano

Lac Vert (LVE), i.e., Green Lake, is located west of Goma city and ~2 km north of the Lake Kivu shoreline (Fig. 1). Lac Vert volcanic rocks possess a Nyiragongo-like, silica-
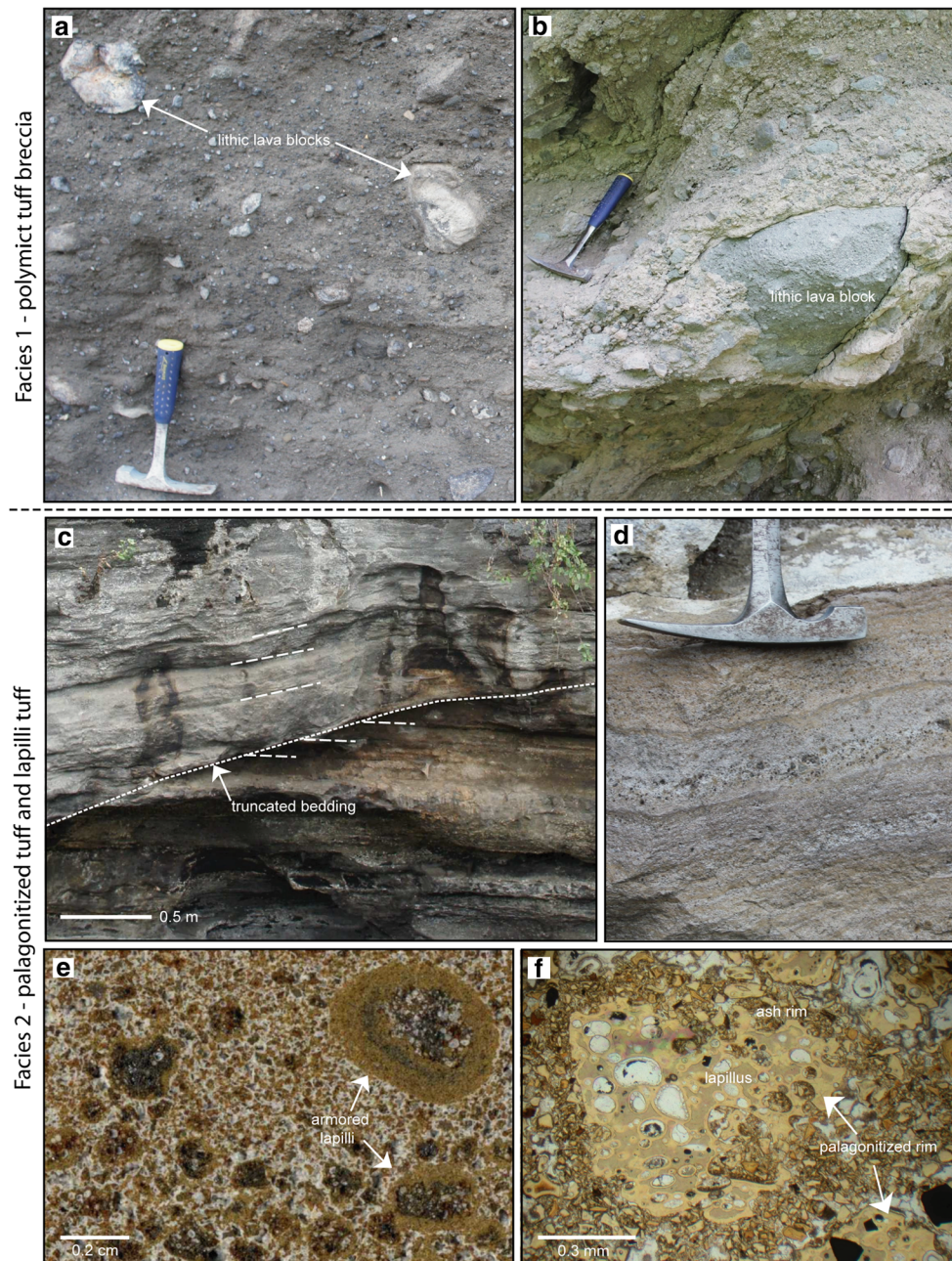

Fig. 2 Lithofacies identified in the small eruptive centers on the northern shoreline of Lake Kivu. Outcrop coordinates are listed in Supplementary Table S1. Facies 1: **a** chaotic polymict tuff breccia at Lac Vert (LVE02); **b** crudely bedded polymict tuff breccia with a meter-sized rounded lithic lava block at Lac Vert (LVE27). Facies 2: **c** large-scale cross-bedding in dilute PDC deposits at Mt. Goma, the dashed line indicates a truncated surface (MGO44); **d** consolidated tuff and lapilli tuff at Buhimba (BUH11); **e** thin section (plane polarized light) of armored lapilli and ash aggregates in Mt. Goma tuffs (MGO08101); **f** characteristic ochre-colored palagonitized armored lapillus in thin section (MGO08101). Facies 3a: **g** decimeter-sized lithic block with impact sag in Mt. Goma tuff (MGO070); **h** decimeter-scale channel, indicated by the dashed line, created by a dilute PDC in Lac Vert tuff (LVE15). Facies 3b: **i** moderately consolidated tuff and lapilli tuff at Nzulu—pig for scale (NZU05); **j** scoriaceous beds in Mt. Goma tuff and lapilli tuff with a vesicular bomb (MGO072). Facies 4: **k** cone-forming scoria deposits at Ndosho (NDO01); and **l** welded spatter with crystalline basement xenoliths at Ndosho (NDO09)
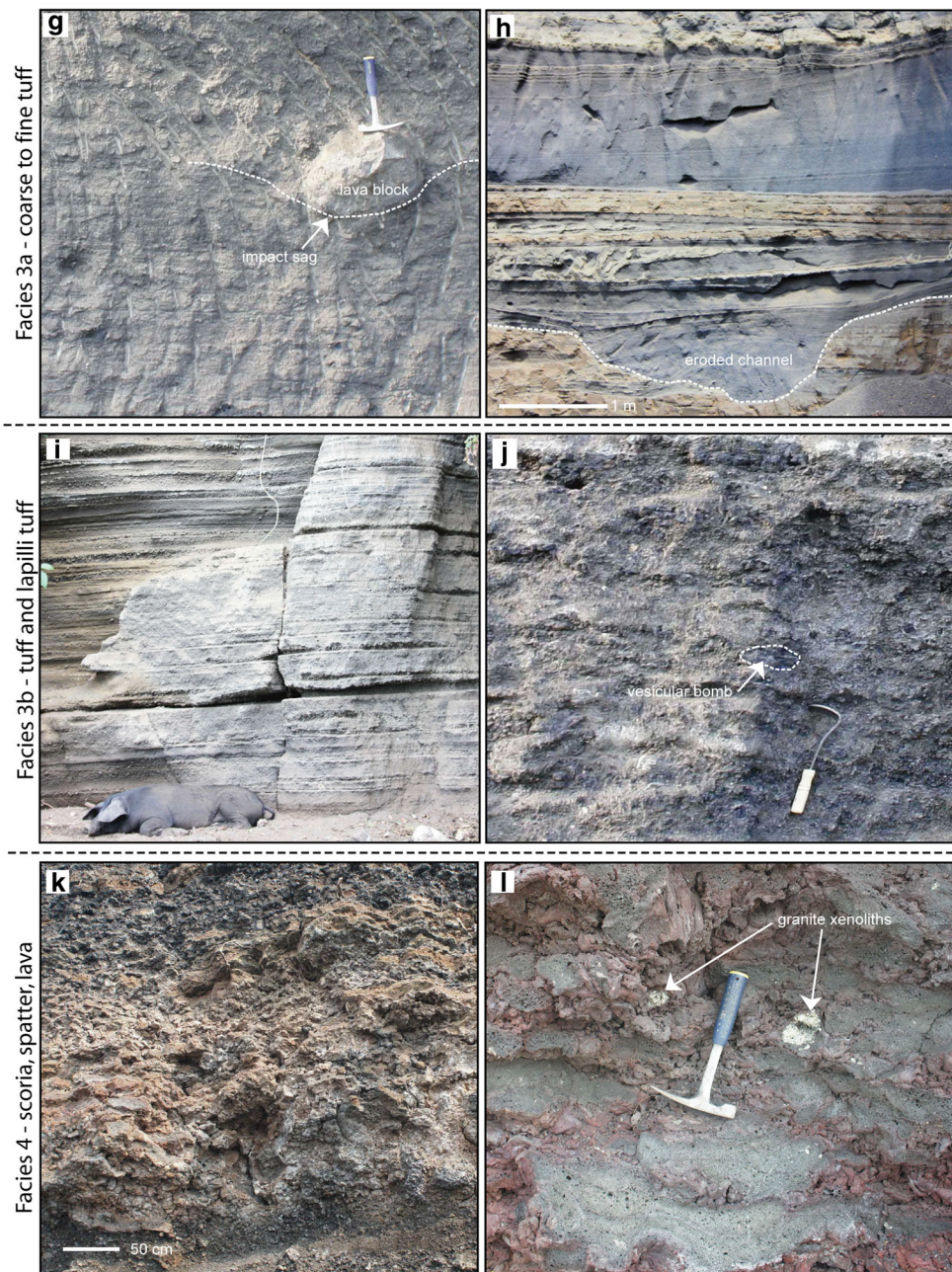
Facies 3a - coarse to fine tuff

lava block

impact sag

eroded channel

1 m

Facies 3b - tuff and lapilli tuff

vesicular bomb

Facies 4 - scoria, spatter, lava

50 cm

granite xenoliths

Fig. 2 (continued)

undersaturated foidite composition, but with lower alkali concentrations than those of Mt. Goma (Chakrabarti et al. 2009). Lac Vert classifies as a maar complex, formed by three craters and an adjacent tephra ring, with the floor of its largest lake-occupied crater lying below the surrounding topography (Fig. 6). The complex has a WSW-ENE elongated shape and scalloped rim, which is breached in the northern and southeastern parts. Three major eruptive phases were discriminated (Fig. 7):

Phase LVE-P1 originated from the southern inundated crater, as suggested by the crater-outward bedding dip (Fig. 6), and consists of two subunits (Fig. 7). LVE-P1-1 is exposed in

the eastern crater cliff and is a facies 1 polymict tuff breccia consisting of millimeter- to meter-sized crystal-rich lithic blocks from pre-LVE lava flows with a minor amount of rounded and elongated pebbles, possibly sourced from an ancient river bed below the volcanic rocks (Figs. 2a and 7a). The fine-grained matrix consists of ~50 vol% submillimetric vesicular lapilli and vitric juvenile ash and ~50 % subangular lithic clasts from pre-LVE lava flows and the crystalline basement. This non-bedded tuff breccia grades upward into the LVE-P1-2 facies 2 consolidated, cross-bedded, and palagonitized tuffs and lapilli tuffs with block impact sags and armored lapilli (Figs. 2d and 7b). The top portion of

Fig. 3 Pléiades 2013 image (2 m resolution) laid over a TanDEM-X-derived hillshade relief image (Albino et al. 2015) of the Mt. Goma tuff cone complex (MGO; location in Fig. 1). Outside the cone base (*red dashed line*), the phreatomagmatic tuffs are masked by more recent lava flows from Nyiragongo
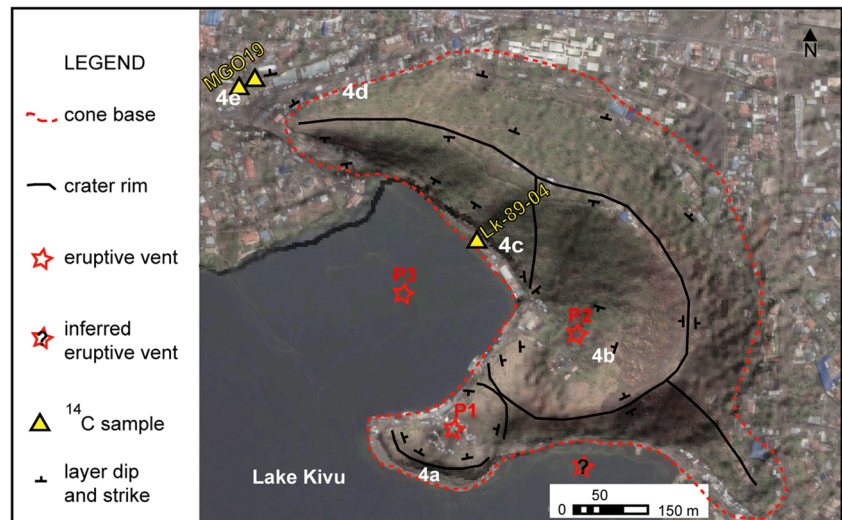
LVE-P1-2 is exposed in the easternmost quarries and its yellow-orange color is ascribed to pervasive alteration (Fig. 7c).

Phase LVE-P2 was sourced from the northern crater with a diameter of 300–400 m as suggested by the surrounding bedding dip orientations (Fig. 6). The 2–15-m-thick facies 3a coarse and fine tuffs are found on top of LVE-P1 over the entire edifice (Figs. 2h and 7c, d). The rocks of this facies are quarried as construction sands. Vertical 10–30-cm displacements of the LVE-P2 beds along small normal faults occurred on the steep slopes of the LVE-P1 upper surface. We infer these displacements are syn-depositional since they terminate within portions of the sequence and never affect the entire sequence.

Phase LVE-P3 is spatially limited to the 80 by 100 m wide crater nested within the larger northern crater (Fig. 6). LVE-P3 is a small-volume facies 1 polymict tuff breccia and contains massive lava blocks of pre-LVE origin, incorporated in a crudely bedded fine gray ash matrix, which consists of ~50 vol% juvenile vitric ash and ~50 % lithic clasts from pre-LVE lava flows and the crystalline basement (Fig. 2b). Its discordant position against the intra-crater wall of LVE-P1-2 tuffs and the absence of LVE-P2 tephra in the LVE-P3 crater itself suggests that LVE-P3 represents the most recent eruptive phase of the Lac Vert complex.

Fossil shells found burrowed in situ in the weathered upper few centimeters of LVE-P1 at the easternmost outer flank were determined as the terrestrial gastropod *Limicolaria* sp. *Schumacher* (Van Damme, personal communication; Crowley and Pain 1970). One shell yielded a radiocarbon age of 1024 ± 43 a cal. BP (13LVE240202a; Table 1; Fig. 5), whereas the surrounding paleosol yielded 2124 ± 78 a cal. BP (13LVE240202b). At the same stratigraphic but intra-crater position below LVE-P2, a paleosol sample in the top of LVE-P1 yielded an age of 2334 ± 37 a cal. BP (13LVE1402). Both paleosol ages define a minimum LVE-P1 eruptive age range of ca. 2380–2000 a (Fig. 5), while the age of the

Limicolaria shell constrains the maximum eruptive age range of the overlying LVE-P2 at ca. 1175–950 a.

A small ~20 m long, ~30-m-wide pahoehoe lava flow lobe invaded Lac Vert in its easternmost corner (Fig. 6), but field relations could not establish if it is part of the LVE complex, or of a more recent lava flow. The entire outer base of the LVE edifice is covered by 1–3-m-thick lava flows. Two samples from the paleosol below a post-LVE lava flow in the eastern breach (Fig. 7d) yielded ages of 378 ± 48 and 382 ± 47 a cal. BP, respectively (13LVE1301 and 13LVE1201; Fig. 5). Two paleosol samples taken below a lava flow covering the NNE slopes yielded ages of 608 ± 35 and 638 ± 40 a cal. BP (13LVE1002a and 13LVE1002b, Fig. 5). These four samples most likely date two separate lava flows to expected age ranges of ca. 465–295 and 685–555 a, respectively. The latter age provides a minimum eruptive age for LVE-P2 as well.
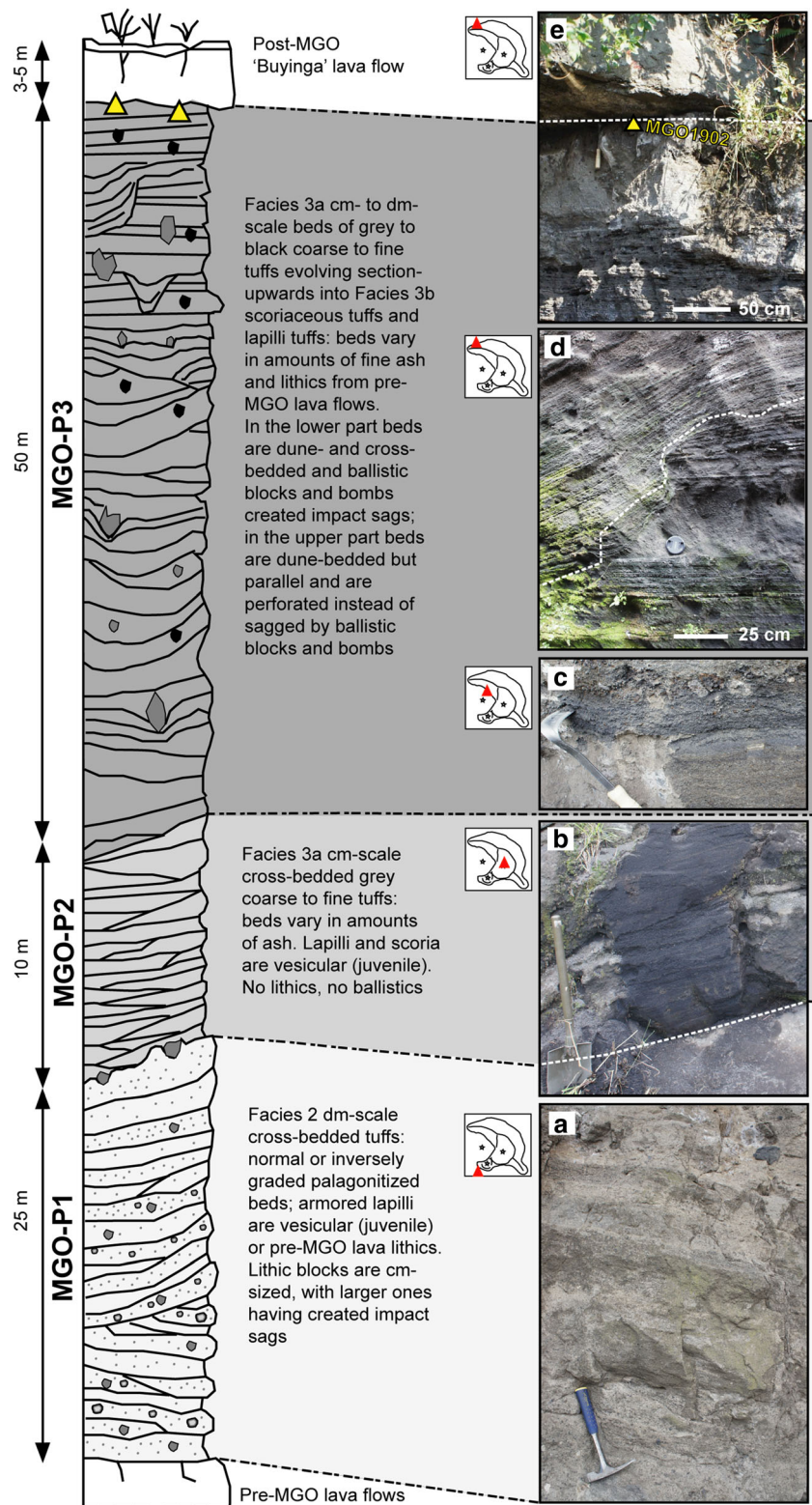
Based on our field and chronological constraints, we infer that LVE-P1 was emplaced before ca. 2380–2000 a. Eruptive phase LVE-P2 then occurred at ca. 1175–550 a, after an approximate hiatus of 800 to 1800 years (Fig. 5).

Other tuff cones

Buhimba and Nyabyunyu tuff cones

Buhimba and Nyabyunyu are two coalesced tuff cones in the Bulengo area (Figs. 1c and 8a). Different names for these cones have been used in the past, which has led to confusion with the Nyarutshiru tuff cone which lies to the East (Thonnard et al. 1965; Denaeyer 1975). A steep escarpment in the lake-side flank of Buhimba delineates an ancient landslide. A secondary but unclear crater may exist at Nyabyunyu (Fig. 8a). Nyarutshiru and Buhimba mainly consist of consolidated facies 2 tuffs and lapilli tuffs (Fig. 2d), while the exposed uppermost deposits of Nyabyunyu are alternating facies

Fig. 4 Lithostratigraphic column of the Mt. Goma deposits dividing the stratigraphic sequence into three eruptive phases. Phreatomagmatic phase **MGO-P1** with facies 2 tuffs originates from the SW on-land crater: **a** decimeter-scale beds of ochre ash tuffs in the eroded lake-facing cliff, with light-gray, centimeter-sized and angular lithic clasts from pre-MGO lava flows—hammer for scale (MGO44). Phreatomagmatic phase MGO-P2 facies 3a tuffs originate from the NE on-land crater: **b** contact between the indurated facies 2 ash tuffs of MGO-P1 and the facies 3a centimeter-scale cross-bedded laminae of mildly indurated dark-gray slightly vesicular coarse tuffs of MGO-P2—shovel for scale (MGO56). Phreatomagmatic phase MGO-P3 produced the most voluminous deposits with alternations of facies 3a and 3b tuffs and the inferred source was in the flooded largest crater: **c** sequence of decimeter-scale subunits with clast-supported laminae, with contrasting median grain size and proportions of fine ash; note the angular lithics from pre-MGO lava flows and the scoriaceous coarsest fraction (MGO64); **d** chute-and-pool structure cut by a fine-grained bedded PDC deposit within the parallel-bedded centimeter-scale laminae of finer and coarser juvenile ash of MGO-P3; fine ash constitutes <1 % here (MGO18). **e** Top of the MGO sequence at its northwestern, most distally exposed side, with paleosol sample MGO19020201, covered by more recent lava of the Buyinga flow (Thonnard et al. 1965)


Post-MGO 'Buyinga' lava flow

Facies 3a cm- to dm-scale beds of grey to black coarse to fine tuffs evolving section-upwards into Facies 3b scoriaceous tuffs and lapilli tuffs: beds vary in amounts of fine ash and lithics from pre-MGO lava flows.
In the lower part beds are dune- and cross-bedded and ballistic blocks and bombs created impact sags; in the upper part beds are dune-bedded but parallel and are perforated instead of sagged by ballistic blocks and bombs

Facies 3a cm-scale cross-bedded grey coarse to fine tuffs: beds vary in amounts of ash. Lapilli and scoria are vesicular (juvenile). No lithics, no ballistics

Facies 2 dm-scale cross-bedded tuffs: normal or inversely graded palagonitized beds; armored lapilli are vesicular (juvenile) or pre-MGO lava lithics. Lithic blocks are cm-sized, with larger ones having created impact sags

Pre-MGO lava flows

3a coarse and fine tuff with some highly vesicular facies 3b scoria beds (see Supplementary materials).

Several open fractures affect the southern flank of Nyarutshiru and the southeastern part of Buhimba. Aligned with these fractures, a NNE-SSW-oriented fissure produced a small-volume spatter cone and adjacent pahoehoe lava flow at the foot of Buhimba and partially vegetated scoriaceous spatter levees in the crater of Buhimba (Fig. 8b). This effusive event therefore post-dates the eruptions that constructed Nyarutshiru and Buhimba.

Fig. 5 Age probability distributions at 95.4 % (2σ) confidence interval for paleosol, charcoal, and shell samples from selected phreatomagmatic and lava flow deposits along the northern shoreline of Lake Kivu (Table 1; sampling locations in Table S1). Samples collected between a tuff deposit and a more recent lava flow simultaneously provide a maximum lava flow age and a minimum age of the phreatomagmatic event
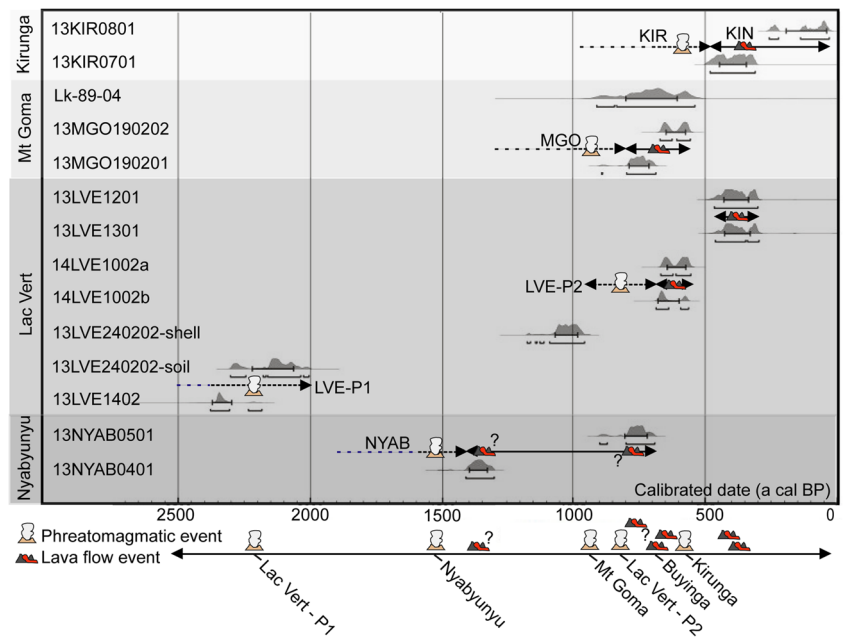
Two paleosol samples taken in the tuff immediately underneath the lava flow which invaded the open craters of Nyabyunyu yielded discordant ages of 761 ± 42 and 1365 ± 34 a cal. BP (13NYAB0501 and 13NYAB0401; Table 1; Figs. 5 and 8c). The minimum eruptive age of Nyabyunyu and the post-Nyabyunyu lava flows is therefore ca. 1400–700 a.

Kirunga tuff cone and Kinungu lava cone

Kirunga is a tuff cone to the SW of Buhimba-Nyabyunyu (Fig. 1c). Only the uppermost part of its deposits is exposed, displaying bedded facies 3a coarse and fine tuff (Fig. 8d, e). To its immediate NW lies Kinungu, called Kirunga II by Denaeyer (1975). Kinungu is a cone of facies 4 welded spatter, similar to that shown in Fig. 2l. A NE-SW-oriented eruptive fissure runs from the southwestern foot of Kinungu towards the small-volume

Kinyogoti tuff cones (Fig. 8d), where it is associated with scoriaceous spatter levees and conelets overlapping the tuff cones. It is however not clear whether the fissure is related to the Kinungu eruption or post-dates it. A lava flow poured out from Kinungu to the NNW into the Bulengo area (Fig. 8d). Two paleosol samples collected in the tuffs near the northwestern base of Kirunga, below the Kinungu lava flow (Fig. 8d, e), yielded radiocarbon ages of 395 ± 51 and 117 ± 77 a cal. BP (13KIR0701 and 13KIR0801; Table 1; Fig. 5). More lithofacies details can be found in the Supplementary materials.

Other small eruptive centers along Lake Kivu's northern shoreline were identified as "hyaloclastite cones" by Denaeyer (1975) and sampled by Capaccioni et al. (2003). We confirm the nature of the following eruptive centers in the field (Fig. 1c; Supplementary materials): facies 2 tuffs and lapilli tuffs at the Bulengo cone and the Kabutembo tuff ring; facies 3a coarse and fine tuffs at the penultimate

Fig. 6 Pléiades 2013 image (2 m resolution) laid over a TanDEM-X-derived hillshade image (Albino et al. 2015) of the Lac Vert maar complex with its surrounding tuff ring (LVE; location in Fig.1). Outside the maar ejecta ring base, the tuffs are covered by more recent lava flows
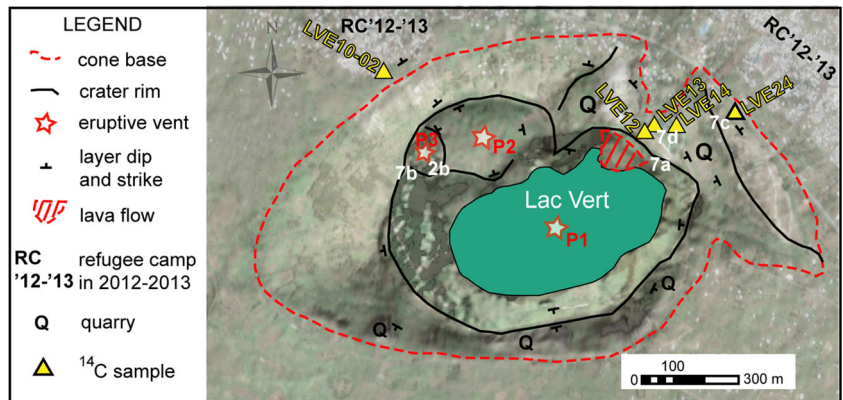
Fig. 7 Lithostratigraphic column dividing Lac Vert into deposits from three eruption phases observed in the field. The first-phase deposit LVE-P1 is composed of a lower facies 1 LVE-P1-1: **a** chaotic breccia tuff composed of gray fine ash with polymict millimeter- to decimeter-sized angular lithics from pre-LVE lava flows and basement rocks (*LVE02*; see also Fig. 2a) and an upper phreatomagmatic facies 2-bedded LVE-P1-2: **b** decimeter-scale beds of palagonitized facies 2 tuff with ~10 % centimeter-sized lithics and >25 % vesicular ash-coated lapilli and ash aggregates—hammer for scale (*LVE26*). The second Facies 3a phreatomagmatic deposit LVE-P2 is found around the northern crater (see also Fig. 2h): **c** contact between the weathered top of LVE-P1 and the facies 3a phreatomagmatic tuff of LVE-P2 with terrestrial gastropod shells, genus *Limicolaria* (*LVE240201*; Table 1). A third small-volume eruptive phase LVE-P3 formed an ejecta ring of facies 1 breccia around a ~20-m-wide crater nested within the northern LVE crater. **d** More recent basaltic lava flows cover the LVE-P2 tuffs, the orange-brown boundary between the two is a thin paleosol (*LVE12-LVE13*; Table 1)
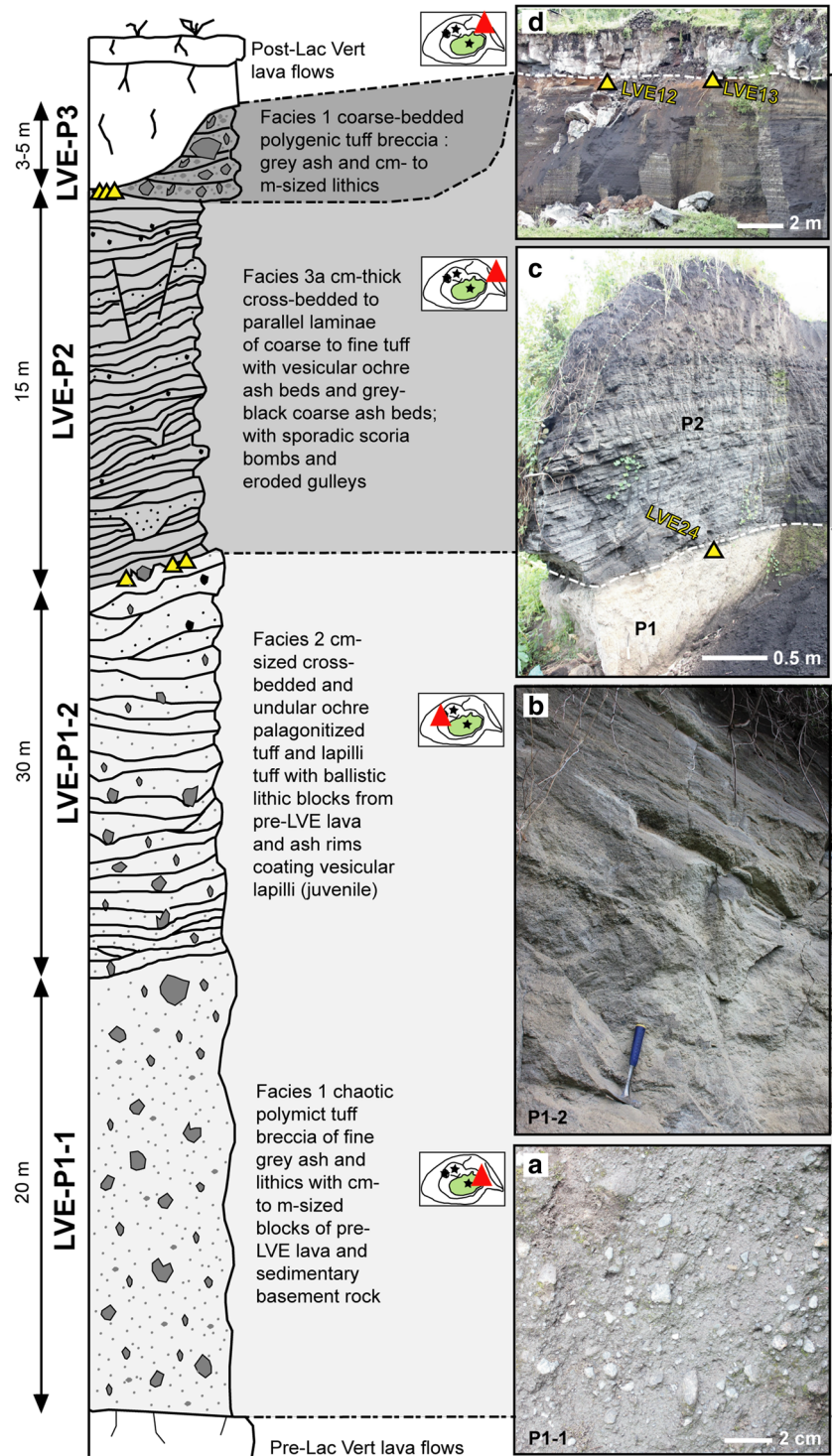

phase of Kashaka; facies 3b ash-and-lapilli tuffs at Nzulu and Kabazana tuff cones, within the Nyamulagira lava flow field (Fig. 2i); and facies 4 magmatic lapilli and scoria at Ndosho and Nengo cones and the uppermost unit of Kashaka (Fig. 2k-l).

Descriptions of hyaloclastite deposits by Denaeyer (1975) resemble our facies 2 palagonitized tuffs and lapilli

tuffs at seven eruptive centers to which access was restricted in 2013 (Fig. 1c): the Kituharu, Kabazana, and two Kinyogoti tuff cones, Tshegera in Lake Kivu, the Bushibu tuff ring, and the lowermost phase of Kashaka. This results in a total of 24 individual phreatomagmatic vents identified at 15 small eruptive centers along the shoreline of Lake Kivu.

Fig. 8 **a** TanDEM-X derived hillshade relief image (Albino et al. 2015) of the aligned cones Nyarutshiru, Buhimba and Nyabyunyu (location in Fig.1c) with the locations of paleosol samples NYAB04 and NYAB05 (Table 1). **b** Small-volume pahoehoe lava flow from a fissure in the eastern flank of Buhimba, correlated to the spatter levees inside the Buhimba crater (BUH02). **c** Location of paleosol sample NYAB04 at the contact between late-eruptive coarse to fine ash beds of the Nyabyunyu tuff cone and its post-eruptive crater-filling lava flow. **d** Hillshade relief image of the Kirunga tuff cone, smaller Kinyogoti tuff cones with a nested eruptive fissure and associated spatter levees, and the Kinungu spatter cone and lava flow (location in Fig.1c). **e** Contact between the Kirunga coarse to fine tuffs and the Kinungu lava flow and location of paleosol sample KIR070201
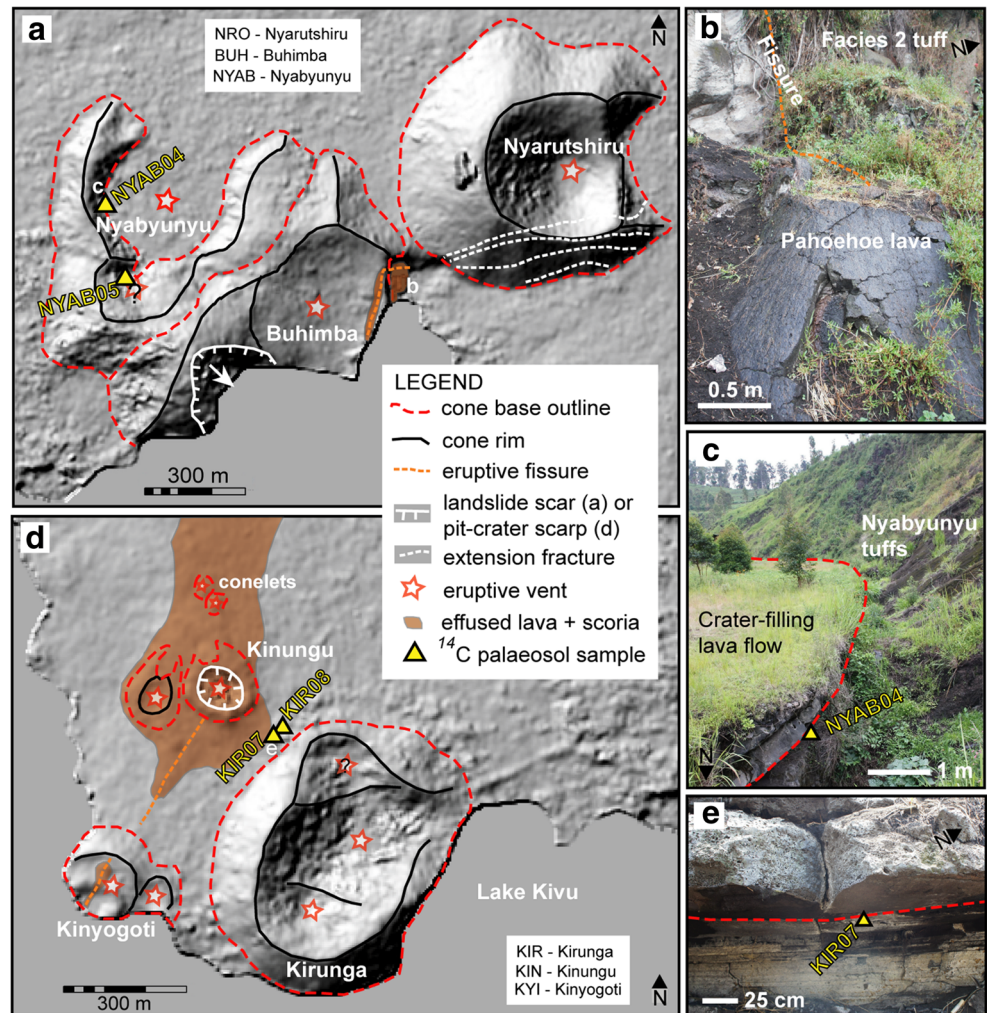
Discussion

Eruption mechanisms

Contrasting eruption mechanisms formed the observed phreatomagmatic and magmatic facies (Table 2 and Fig. 2):

Facies 1 polymict tuff breccias consist partially of poorly sorted non-vesicular and subangular volcanic clasts with abundant microcrystals and partially of vesicular vitric fine to coarse ash. We infer the former are accidental lithics from violently excavated bedrock, while the latter are juvenile clasts (Fig. 2f). This facies was therefore generated by explosive blasting through the bedrock during the vent opening phase of the eruption, while the ascending magma reacted with the aquifer in the volcanic rocks close to Lake Kivu.

Facies 2 tuffs and lapilli tuffs contain ash aggregates, armored lapilli, impact sags below ballistic blocks, and have a high consolidation grade, all of which suggest the presence of liquid water in the eruption column and deposits. The initial magma may have contained enough magmatic volatiles to drive fragmentation and create vesicular pyroclasts.

However, the influx of external water into the system likely enhanced fragmentation into abundant fine ash and leading to near-source fallout of ash particles due to wet aggregation (Koyaguchi and Woods 1996). The large-scale cross-laminations, pinch-and-swell, and dune-bedded structures are similar to those described by Brand and Clarke (2012) at the Table Rock Complex, Oregon, USA, and are consistent with the occurrence of erosive high-energy PDC events, thought to have formed at vents below or at lake level. The input of water into the vent needs to be sufficiently high and the magma ascent rate sufficiently low, or the temperature of the propagating dilute PDC needs to decrease enough relative to the temperature at the vent, in order to generate the typical depositional characteristics (Fisher and Schmincke 1984; Branney and Kokelaar 2002).

Facies 3 semi-consolidated clast-supported tuff and lapilli tuff dominantly comprise juvenile coarse ash and small lapilli. The small amount of fine ash (<1 %) in facies 3a and sagged beds below sporadic decimeter-scale lava lithic blocks and vesicular scoria bombs are suggestive of magma-water interaction and the presence of external water, which is however less

pronounced than in facies 2 deposits. The magma-water interaction for facies 3a is nevertheless inferred to have been more efficient than during emplacement of near-magmatic facies 3b, during which were formed scoriaceous fine lapilli beds and a dominance of coarse ash beds, perforated rather than sagged by highly vesicular bombs. Cross-laminations, syn-eruptive erosion channels and chute-and-pool structures occur at a smaller scale than in facies 2. Brand et al. (2014) have shown that lower amounts of liquid water in the eruption column could lead to PDCs with a lower bulk density and thus shorter run-out distances. Additionally, the syndepositional displacements of some portions of LVE-P2 are consistent with a humid nature of the freshly deposited facies 3 tephra, which failed by gravitational slip on the steep underlying LVE-P1 slopes.

Facies 4 dry magmatic deposits were sourced from fissures observed at Buhimba and Kinungu (Fig. 8). As these lava flows and spatter levees cover the phreatomagmatic tuffs, the former must have erupted more recently than the cone-forming eruptions.

The lithofacies sequence at Mt. Goma indicates an overall evolution from an explosive and water-rich eruption stage into water-poor or even dry eruption stages. The initial phreatomagmatic vents likely became sheltered from Lake Kivu's surface water by the growing tuff cone, similar to, e.g., Surtsey (White and Houghton 2000). At Lac Vert, the proximity of Lake Kivu water, possibly in an aquifer, played a dominant role in the first eruptive phase, while it only contributed water to a limited extent to the active vent of the second phase 800–1800 years later. Such interactions with the aquifer or surface water and other eruption factors are difficult to constrain however, as illustrated, e.g., in the complex sequence of magmatic and phreatomagmatic facies at Mt. Gambier, Newer Volcanic Province, Australia (van Otterloo et al. 2013).

Chronology of lake-level fluctuations and phreatomagmatic eruptions

The chronology of Lake Kivu water-level variations was recently reconstructed from morphological analysis of current lake bathymetry combined with sedimentation rate estimates, radiocarbon dating, and bio-chemical proxies in lake sediment cores. These suggest that the level of Lake Kivu was 380 m below its current level at ~12.2 ka and rose to 100 m above the current level in a few thousands (Ross et al. 2014; Zhang et al. 2014) to as little as 200 years (Wood and Scholz 2016). The rapid lake-level rise is attributed to either (1) damming of the outflow of Lake Kivu to the North by VVP volcanism, subsequently forcing its drainage by the Ruzizi river to the South from ~9.7 ka (Ross et al. 2014; Zhang et al. 2014) or (2) wetter climate conditions, which affected all neighboring East African Rift lakes and resulted in a more rapid response time of the lake level than could be expected from the relatively slow build-up of the lava flow delta from VVP volcanism

(Wood and Scholz 2016). During the Holocene, the water level of Lake Kivu then dropped gradually to its current level. The +100-m lake-level high-stand must post-date the 11,972 ± 221-a cal. BP eruption that constructed the dry magmatic Nengo scoria cone which lies at the elevation of the current lake level of ~1463 m a.s.l. (Lk-89-02; Table 1; Fig. 1c; Tuttle et al. 1990).

Higher Lake Kivu stands must have shifted the northern shoreline northward in the Holocene, towards Nyamulagira and Nyiragongo, and established shallow lake water or shallow aquifers at the existing eruptive centers. The occurrence of explosive magma-water interaction is thus in the first order controlled by the availability of external water controlled by Lake Kivu-level fluctuations.

In addition to lake-level fluctuations, the varying explosivity and efficiency of the magma-water interaction may have been partly controlled by varying magma ascent rates and magma volatile contents between contrasting eruption phases (e.g., Németh et al. 2012; Valentine et al. 2013). Geochemical composition of the magma on the other hand does not seem to have affected the eruption styles, because little differences were found between the different eruptive centers (Cappacioni et al. 2003; Chakrabarti et al. 2009; Barette et al. 2016). Such combination of eruptive and environmental controls could explain the spatial concurrence of dry magmatic and phreatomagmatic centers in the proximity of abundant (aquifer-confined) water of Lake Kivu in the Lac Vert-Bulengo area.

Overall, the occurrence of phreatomagmatism only within ~4 km from the current Lake Kivu's shoreline strongly suggests the process was mainly controlled by the presence or proximity of Paleo-Lake Kivu. We thus suggest that all of the identified phreatomagmatic vents must have become active after the lake-level rise since ~12.2 ka, with some of them forming in shallow water conditions when the level of Lake Kivu was higher than the current level. Our radiocarbon dates are consistent with such Holocene eruptive ages.

The generally poorly developed paleosols on top of the phreatomagmatic deposits suggest a maximum timespan of 200–500 years between the eruptive phases and subsequent covering by lava flows, taking into account the rapidity of paleosol formation in a tropical climate (James et al. 2000). We infer that the three phreatomagmatic phases of Mt. Goma succeeded one another within the same eruptive episode or a few hundred years at maximum, considering they are separated from each other by sharp contrasts in consolidation and facies type, but without evidence of paleosol development. At Lac Vert, a gastropod shell yielded a calibrated age ca. 800–1000 a younger than the well-developed paleosol in the top of LVE-P1 in which it was found (Table 1; Figs. 5 and 7). This represents a time gap between on one hand the end of the LVE-P1 eruption and onset of paleosol formation and on the other hand the death of the gastropod and burial of its shell

within the paleosol. In such manner, the age of LVE-P2 is constrained between the gastropod age and the age of the overlying lava flows, ca. 800–1800 years after LVE-P1 (Table 1; Fig. 5). At Nyabyunyu, the discrepancy between radiocarbon dates of the same paleosol developed onto the phreatomagmatic deposits (Fig. 5) could be due to (1) an age difference between the smaller and larger crater, i.e., two separate phreatomagmatic events or (2) the invasion of two separate lava flows 500–600 years apart. Furthermore, several sources of uncertainty may affect the obtained radiocarbon dates, such as the mixed-age nature of paleosols versus single charcoal fragments or shell material, contamination by more recent organic material or an "aging" influence of local volcanic CO_2 degassing (Calderoni and Turi 1998). Despite these potential complications, most of our radiocarbon dates are broadly consistent with each other and with their stratigraphic positions (Fig. 5).

Our radiocarbon dates suggest the occurrence of at least five phreatomagmatic eruptions within the last 2.5 kyears, accounting for an average recurrence rate of ~500 years (Fig. 5; Mt. Goma, Lac Vert P1, Lac Vert P2, Kirunga, and Nyabyunyu). Additionally, we identify five lava flow events (Fig. 5). Four pre-historical lava flows, most likely sourced from the southwestern fissure zone of Nyiragongo, were emplaced in the Bulengo area within the last ~1.5 kyears. This finding is of specific interest because no lava flows from Nyiragongo have impacted that area during the past ~150 years.

Finally, we also constrain an eruptive age of ca. 1.0–0.8 ka for the Buyinga lava flow, sourced from the N-S-oriented fissure zone extending from the main crater of Nyiragongo to the northern flanks of Mt. Goma and Lake Kivu (Thonnard et al. 1965). This immediately constrains a minimum eruptive age of the Mt. Goma eruptions. At least one of both events coincided temporally with the formation of the 765-a cal. BP unusually organic-rich layer encountered in lake sediment cores. Ross et al. (2015) suggest that this layer is the result of a lake mixing event induced by a volcanic eruption which occurred on the lake shore or on the lake floor and disrupted the lake water stratification. At present we do not have sufficient evidence to suggest a causal link between the Mt. Goma eruption(s) and the lake-mixing event, but our findings provide further insight into potential triggers for lake stratification destabilization. Considering the high population density close to the lake, the chronology of subaerial and sublacustrine eruptions deserves further scientific attention, as do the potential links between subaerial and sublacustrine volcanism and limnic eruptions in the Lake Kivu area.

Spatial pattern of magma-water interaction

Figure 9 shows a compilation of the 24 phreatomagmatic vents that were identified at 15 phreatomagmatic eruptive centers. This number of phreatomagmatic vents is similar to the amount of individual tephra layers identified in lake sediment cores spanning the last ~10 kyears, and broadly confirm a recurrence of phreatomagmatic eruptions every ~500 years in the area (Wood and Scholz 2016). All the vents can be found within a ~4-km distance from the present shoreline of Lake Kivu, twice as far as previously recognized by Denaeyer (1975) and Capaccioni et al. (2003). Additionally, the NE-SW and N-S fissure networks of Nyiragongo volcano indicate two areas of relatively high eruptive susceptibility between Nyiragongo and the northern part of Lake Kivu (Capaccioni et al. 2003; Chakrabarti et al. 2009).

Magma is able to either ascend vertically directly below the shoreline or migrate laterally through the fissure networks away from Nyiragongo towards the lake shore. We identified an undated small-volume lava flow from a fissure which opened in the Buhimba cone a few tens of meters from the present Lake Kivu shoreline (Fig. 8a, b). The NE-SW orientation of this fissure is consistent with that of the southwestern Nyiragongo fissure network (Smets et al. 2016). During the 2002 Nyiragongo eruption, a series of eruptive fissures opened on the southern flank and a shallow intrusion propagated southwards to Goma. One of the two lava flow branches reached the shoreline without interacting violently with the lake waters (Lorke et al. 2004). Ground deformation data nevertheless suggested a dissociated second deeper intrusion which extended southward beneath the floor of Lake Kivu (Wauthier et al. 2012). Additionally, several tuff rings and maars lie on the lake floor, up to a few kilometers South of the lake's northern shoreline, at a depth of 200–300 m below the current water level, and were formed as the result of subaerial or shallow lacustrine eruptions that occurred during lake-level lowstands, i.e., before ~12.2 ka (Ross et al. 2014; Fig. 9). The spatial distribution of these subaqueous vents shows similar alignments than those observed in the Bulengo area. We infer that a 2002-like shallow magmatic intrusion close to Lake Kivu could either result in a dry magmatic eruption or explosive magma-water interaction, while a 2002-like deep intrusion event has the potential to open a vent below the lake floor, with an unknown effect on the lake stratification and the subaerial environment (e.g., Mastin and Witter 2000). No such volcanic event has been experienced in the past 150 years in the Sake-Goma-Gisenyi urban area.

Dilute PDC hazard implications

Facies 2 and 3 deposits of Mt. Goma and Lac Vert indicate that dilute PDC events of varying intensities have occurred in the past. While the impact of tephra fallout from these relatively small-volume phreatomagmatic eruptions is mostly limited to static loading by wet ash and potential failure of buildings and infrastructure, the lateral impact of ground-hugging and rapidly moving PDCs represents another severe hazard (e.g., Wilson et al. 2014).
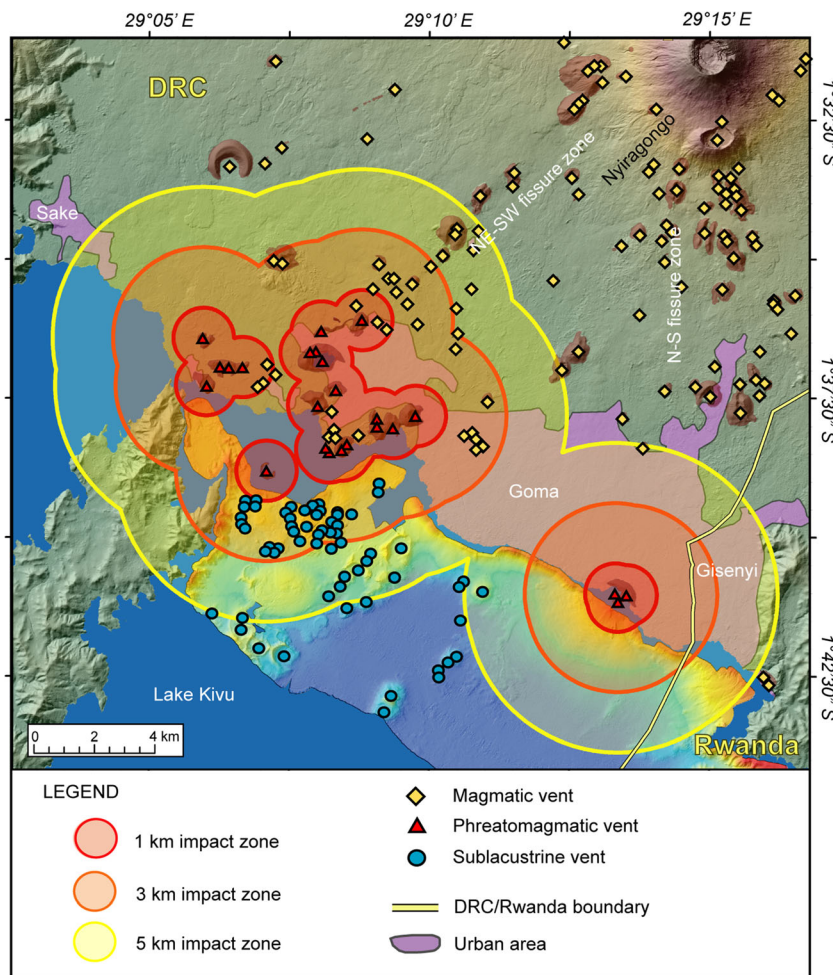
Fig. 9 Spatial extent of the area potentially impacted in the past by more cohesive (1 km extent) or more dilute (5 km extent) PDCs from past phreatomagmatic eruptive vents in the Sake-Goma-Gisenyi urban area as identified in the field and from the literature (background: TanDEM-X DEM hillshade image from Albino et al. 2015; Lake Kivu bathymetry from Ross et al. 2014). All marked subaerial phreatomagmatic vents (red triangles) are inferred to be of Holocene age, while the currently sublacustrine tuff rings and cones (*blue dots*) are assumed to have formed during periods of lower lake levels before ~12.2 ka (Ross et al.

2014). Note that when combined, the high-intensity PDC impact zones within 5 km around each identified vent comprise almost the entire currently urbanized area. The impact and spatial extent of PDCs (and ash fall) during a potential future phreatomagmatic eruption in the urban area would depend on the future vent location, eruption intensity and duration, and wind direction. This map presents a qualitative estimation of the total area that may have been impacted in the past by phreatomagmatic deposits from small eruptive centers and should not be interpreted as a probabilistic hazard map

We did not observe the full extent of the phreatomagmatic deposits since they are covered by more recent lava flows. The depositional facies of the dilute PDC deposits and the overall magma compositions of the Virunga rocks (Barette et al. 2016) are nevertheless broadly similar to those of well-studied surge deposits of the Auckland Volcanic Field (AVF), New Zealand (e.g., Brand et al. 2014; Agustin-Flores et al. 2015). Allen et al. (1996) suggest that AVF cohesive PDCs did not travel further than 1–3 km, while dilute PDCs traveled up to 5 km away from the vent. Taking into account these distances, Fig. 9 presents a buffer map of zones potentially impacted in the Holocene by dilute PDCs and limited ash fallout around the phreatomagmatic vents. The map in Fig. 9 is a qualitative estimation of the total area potentially impacted by phreatomagmatic ash deposits in the past and

should hence not be interpreted as a probabilistic hazard map. Spatial extent of the deposits depends on the vent location, eruption intensity and duration, and wind direction which varies dominantly between NW and SSW in the area (Dingwell et al. 2016). These parameters will also control the emplacement of future deposits.

About half of the present-day Goma-Gisenyi urban area lies within the 3-km impact zone and almost the entire urban area (>1.2 million inhabitants in 2015) lies within the 5-km impact zone (Fig. 9). This VVP case study demonstrates how relatively small volumes of erupting magma interacting with external water can cause explosive events with potentially severe consequences in a region that is otherwise largely dominated by effusive volcanism. If a phreatomagmatic eruption were to occur in the near future close to the Kivu shoreline, the

physical and socio-economic impact could be severe, especially considering the high vulnerability of the conflict-torn population of the East DRC and border region of Rwanda (Michellier et al. 2016).

Conclusions

We provide a stratigraphic description and the first comprehensive Holocene radiocarbon chronology of the phreatomagmatic deposits along the northern shoreline of Lake Kivu:

1. Phreatomagmatic deposits from satellite eruptive centers of Nyiragongo and Nyamulagira volcanoes, along the Lake Kivu shoreline, can be subdivided into three types: Facies 1 polygenetic tuff breccias from vent-clearing explosions, facies 2 palagonitized tuffs and lapilli tuffs from water-rich phreatomagmatic eruptions, and facies 3 coarse and fine lapilli tuffs from medium-wet to near-dry phreatomagmatic eruptions.
2. At least 24 phreatomagmatic events constructed at least 15 phreatomagmatic tuff cones, rings, and maars in the last ~12.2 kyears within a 4-km distance of the current northern shoreline of Lake Kivu. Deposit characteristics suggest that dilute PDC events and ash fallout repeatedly affected most of the presently urbanized area (>1.2 million inhabitants in 2015).
3. New radiocarbon dates indicate the occurrence within the past 2500 years of at least five lava flow events, two of which occurred in the past 500 years, and at least five phreatomagmatic eruptions with centennial to millennial recurrence rates.
4. The Buyinga lava flow from Nyiragongo occurred 1000–800 years ago and was preceded by tens to a few hundred years, by the most recent phreatomagmatic phase of the Mt. Goma cone complex. This age is contemporaneous with that of a lake stratification destabilization event in Lake Kivu identified by Ross et al. (2015).
5. A temporal hiatus of 800–1800 years between the two eruptive phases of the Lac Vert maar volcano suggests that eruptions in "monogenetic" volcanic fields may in fact re-use previously existing magma ascent paths.

Our results encourage consideration of explosive magma-water interaction, or phreatomagmatism, as a likely eruption scenario in the contingency plan and risk management in the cities of Saké-Goma (DRC) and Gisenyi (Rwanda). The new chronological framework and lithofacies analysis of the phreatomagmatic eruptions should be extended, both in terrestrial and sublacustrine environments, to further unravel the range of eruptive mechanisms. This would lead to an improved spatial and temporal susceptibility model for the phreatomagmatic hazard along Lake Kivu's northern shoreline.

References

Agustin-Flores J, Németh K, Cronin SJ, Lindsay JM, Kereszturi G (2015) Shallow-seated explosions in the construction of the Motukorea tuff ring (Auckland, New Zealand): evidence from lithic and sedimentary characteristics. J Volcanol Geotherm Res 304:272–286

Albino F, Kervyn F, d'Oreye N, Smets B (2015) High-resolution TanDEM-X DEM: an accurate method to estimate lava flow volumes at Nyamulagira volcano (D.R. Congo). J Geophys Res: Sol E 120:4189–4207

Allen SR, Bryner VF, Smith IEM, Balance PF (1996) Facies analysis of pyroclastic deposits within basaltic tuff-rings of the Auckland volcanic field, New Zealand. New Zeal J Geol Geophys 39:309–327

Barette F, Poppe S, Smets B, Benbakkar M, Kervyn M (2016) Spatial variation of volcanic rock geochemistry in the Virunga Volcanic Province: statistical analysis of an integrated database. J Afr Earth Scie (in press)

Brand BD, Clarke AB (2012) An unusually energetic basaltic phreatomagmatic eruption: using deposit characteristics to constrain dilute pyroclastic density current dynamics. J Volcanol Geotherm Res 243-244:81–90

Brand BD, Gravley DM, Clarke AB, Lindsay JM, Bloomberg SH, Agustin-Flores J, Németh K (2014) A combined field and numerical approach to understanding dilute pyroclastic density current dynamics and hazard potential: Auckland volcanic field, New Zealand. J Volcanol Geotherm Res 276:215–232

Branney MJ, Kokelaar P (2002) Pyroclastic density currents and the sedimentation of ignimbrites. Mem Geol Soc Lond 27:143

Bronk Ramsey C (2009) Bayesian analysis of radiocarbon dates. Radiocarbon 51:337–360

Calderoni G, Turi B (1998) Major constraints on the use of radiocarbon dating for tephrochronology. Quat Int 47:153–159

Capaccioni B, Vaselli O, Santo AP, Yalire MM (2003) Monogenic and polygenic volcanoes in the area between the Nyiragongo summit crater and the Lake Kivu shoreline. Acta Volcanol 14:129–136

Chakrabarti R, Basu AR, Santo AP, Tedesco D, Vaselli O (2009) Isotopic and geochemical evidence for a heterogeneous mantle plume origin of the Virunga volcanics, East African Rift system. Chem Geol 259:273–289

Crowley TE, Pain T (1970) A monographic revision of the African land snails of the genus Limicolaria Schumacher (Mollusca-

Achatinidae). Annales Musée Royal de l'Afrique Centrale Tervuren, Scie Zoolog 177:1–61

Denaeyer ME (1975) Le glacis des volcans actifs au Nord du Lac Kivu. Mémoires du Museum National d'Histoire Naturelle-Série C-Sciences de la Terre 33:79 pp

Dingwell A, Rutgersson A, Claremar B, Arellano S, Yalire MM, Galle B (2016) Seasonal and diurnal patterns in the dispersion of SO_2 from Mt. Nyiragongo. Atmosph Environ 132:19–29

Ebinger CJ (1989) Tectonic development of the western branch of the East African Rift System. Geol Soc Am Bull 101:885–903

Fisher RV, Schmincke H-U (1984) Pyroclastic rocks. Berlin, Springer-Verlag 472 pp

GA V, RV F (2000) Pyroclastic surges and blasts. In: Sigurdsson H, Houghton B, Rymer H, Stix J, McNutt S (eds) Encyclopedia of volcanoes. Academic Press, San Diego, CA, pp. 571–580

Houghton B, White JDL, Van Eaton AR (2015) Phreatomagmatic and related eruption styles. In: Sigurdsson H, Houghton B, McNutt S, Rymer H, Stix J (eds) The encyclopedia of volcanoes, 2nd edn. Academic Press, San Diego, CA, pp. 571–580

Houghton BF, Wilson CJN, Smith IEM (1999) Shallow-seated controls on styles of explosive basaltic volcanism: a case study from New Zealand. J Volcanol Geotherm Res 91:97–120

James P, Chester D, Duncan A (2000) Volcanic soils: their nature and significance for archaeology. In: McGuire WG, Griffiths DR, Hancock PL, Stewart IS (eds) The Archaeology of Geological Catastrophes. Geol Soc London Spec Publ 171:317–338

Kokelaar P (1986) Magma-water interactions in subaqueous and emergent basaltic volcanism. Bull Volcanol 48:275–289

Komorowski J (2003) The January 2002 flank eruption of Nyiragongo volcano (Democratic Republic of Congo): chronology, evidence for a tectonic rift trigger, and impact of lava flows on the city of Goma. Acta Vulcanol 14:27–62

Koyaguchi T, Woods AW (1996) On the formation of eruption columns following explosive mixing of magma and surface-water. J Geophys Res 101:5561–5574

Lorke A, Tietze K, Halbwachs M, Wüest A (2004) Response of Lake Kivu stratification to lava inflow and climate warming. Limnol Oceanogr 49:778–783

Manville V, Németh K, Kano K (2009) Source to sink: a review of three decades of progress in the understanding of volcaniclastic processes, deposits, and hazards. Sedim Geol 220:136–161

Mastin LG, Witter JB (2000) The hazards of eruptions through lakes and seawater. J Volcanol Geotherm Res 97:195–214

Michellier C, Pigeon P, Kervyn F, Wolff E (2016) Contextualizing vulnerability assessment: a support to geo-risk management in Central Africa. Nat Hazards 82:27–42

Moore JG, Nakamura K, Alcaraz A (1966) The 1965 eruption of Taal volcano. Sci 151:955–960

Németh K, Cronin SJ, Smith IEM, Flores JA (2012) Amplified hazard of small-volume monogenetic eruptions due to environmental controls, Orakei Basin, Auckland volcanic field, New Zealand. Bull Volcanol 74:2121–2137

Pauly BD, Schiffman P, Zierenberg RA, Clague DA (2011) Environmental and chemical controls on palagonitization. Geochem Geophys Geosyst 12:Q12017

Reimer PJ, Bard E, Bayliss A, Beck JW, Blackwell PG, Bronk Ramsey C, Grootes PM, Guilderson TP, Haflidason H, Hajdas I, Hattz C, Heaton TJ, Hoffmann DL, Hogg AG, Hughen KA, Kaiser KF, Kromer B, Manning SW, Niu M, Reimer RW, Richards DA, Scott EM, Southon JR, Staff RA, Turney CSM, van der Plicht J (2013) IntCal13 and Marine13 radiocarbon age calibration curves 0–50, 000 years cal BP. Radiocarbon 55:1869–1887

Ross KA, Schmid M, Ogorka S, Muvundja FA, Anselmetti FS (2015) The history of subaquatic volcanism recorded in the sediments of Lake Kivu, East Africa. J Paleolimnol 54:137–152

Ross KA, Smets B, De Batist M, Hilbe M, Schmid M, Anselmetti FS (2014) Lake-level rise in the late Pleistocene and active subaquatic volcanism since the Holocene in Lake Kivu, East African Rift. Geomorphol 221:274–285

Schmincke H-U, Fisher RV, Waters A (1973) Antidune and chute and pool structures in the base surge deposits of the Laacher See Area, Germany. Sedimentol 20:553–574

Smets B, Delvaux D, Ross KA, Poppe S, Kervyn M, d'Oreye N, Kervyn F (2016) The role of inherited crustal structures in the development of rift segments: insights from the Kivu basin, western branch of the East African Rift. Tectonophys 683:62–76

Smets B, Kervyn M, d'Oreye N, Kervyn F (2015) Spatio-temporal dynamics of eruptions in a youthful extensional setting: insights from Nyamulagira volcano (D.R. Congo), in the western branch of the East African Rift. Earth-Sci Rev 150:305–328

Tazieff H (1977) An exceptional eruption: Mt Niragongo, Jan. 10th, 1977. Bull Volcanol 40:189–200

Thonnard RLG, Denaeyer NE, Antun P (1965) Carte volcanologique des Virunga (Afrique centrale), Feuille no.1, 1:50,000. Centre National de Volcanologie (Belgium), Publication no. 32

Tuttle ML, Lockwood JP, Evans WC (1990) Natural hazards associated with Lake Kivu and adjoining areas of the Birunga Volcanic Field, Rwanda and Zaire, Central Africa-final report. U.S. Geological Survey, Open File Report 90–691

Valentine G, Cortés JA (2013) Time and space variations in magmatic and phreatomagmatic eruptive processes at easy chair (lunar crater volcanic field, Nevada, USA). Bull Volcanol 75:752

Van Eaton AR, Herzog M, Wilson CJN, McGregor J (2012) Ascent dynamics of large phreatomagmatic eruption clouds: the role of microphysics. J Geophys Res 117:B03203. doi:10.1029/2011 JB008892

van Otterloo J, Cas RAF, Sheard MJ (2013) Eruption processes and deposit characteristics at the monogenetic Mt. Gambier volcanic complex, SE Australia: implications for alternating magmatic and phreatomagmatic activity. Bull Volcanol 75:737

Wauthier C, Cayol V, Kervyn F, d'Oreye N (2012) Magma sources involved in the 2002 Nyiragongo eruption, as inferred from an InSAR analysis. J Geophys Res 117:B05411

White JDL, Houghton B (2000) Surtseyan and related phreatomagmatic eruptions. In: Sigurdsson H, Houghton B, Rymer H, Stix J, McNutt S (eds) Encyclopedia of volcanoes. Academic Press, San Diego, CA 495–511

White JDL, Houghton BF (2006) Primary volcaniclastic rocks. Geology 34:677–680

White JDL, Ross P-S (2011) Maar-diatreme volcanoes: a review. J Volcanol Geotherm Res 201:1–29

Wilson G, Wilson TM, Deligne NJ, Cole JW (2014) Volcanic hazard impact to critical infrastructure: a review. J Volcanol Geotherm Res 286:148–182

Wohletz KH (1986) Explosive magma-water interactions: thermodynamics, explosion mechanisms, and field studies. Bull Volcanol 48:245–264

Wood DA, Scholz CA (2016) Stratigraphic framework and lake level history of Lake Kivu, East African Rift. J Afr Earth Scie:1–13

Zhang X, Scholz CA, Hecky RE, Wood DA, Zal HJ, Ebinger CJ (2014) Climatic control of the late quaternary turbidite sedimentology of Lake Kivu, East Africa: implications for deep mixing and geologic hazards. Geology 42:811–814

Zimanowski B, Büttner R, Lorenz V (1997) Premixing of magma and water in MFCI experiments. Bull Volcanol 58:491–495